Chemical and Process Engineering 2014, 35 (1), 35-45
DOI: 10.2478/cpe-2014-0003

CONTRIBUTION OF LIQUID- AND GAS-SIDE MASS TRANSFER COEFFICIENTS TO OVERALL MASS TRANSFER COEFFICIENT IN TAYLOR FLOW IN A MICROREACTOR

Paweł Sobieszuk[1*], Filip Ilnicki[2], Ryszard Pohorecki[1]

[1]Faculty of Chemical and Process Engineering, Warsaw University of Technology, Warynskiego 1, 00-645 Warsaw, Poland

[2]Nalecz Institute of Biocybernetics and Biomedical Engineering, Polish Academy of Sciences, Ks. Trojdena 4; 02-109 Warsaw; Poland

Gas-liquid microreactors find an increasing range of applications both in production, and for chemical analysis. The most often employed flow regime in these microreactors is Taylor flow. The rate of absorption of gases in liquids depends on gas-side and liquid-side resistances. There are several publications about liquid-side mass transfer coefficients in Taylor flow, but the data about gas-side mass transfer coefficients are practically non existent. We analysed the problem of gas-side mass transfer resistance in Taylor flow and determined conditions, in which it may influence the overall mass transfer rate. Investigations were performed using numerical simulations. The influence of the gas diffusivity, gas viscosity, channel diameter, bubble length and gas bubble velocity has been determined. It was found that in some case the mass transfer resistances in both phases are comparable and the gas-side resistance may be significant. In such cases, neglecting the gas-side coefficient may lead to errors in the experimental data interpretation.

Keywords: Taylor flow, mass transfer coefficients, microreactor, CFD simulations

1. INTRODUCTION

Gas-liquid Taylor flow in microreactors finds an increasing range of applications both in production, and for analysis. As examples one can cite: direct synthesis of hydrogen peroxide (Hessel et al., 2005), direct fluorination (Chambers et al., 2001), photochemical gas-liquid reactions (Ehrich et al., 2002), automated screening of reaction conditions (Churski et al., 2010), fast determination of solubility and diffusivity (Abolhasani et al., 2012; Lefortier et al., 2012), etc. In most cases mass transfer in gas-liquid Taylor flow is a liquid-side controlled process, and authors of papers concerning this problem use the liquid-side volumetric mass transfer coefficient, k_La for characterisation of the mass transfer rate. While absolutely correct in the case of poorly soluble gases, or when a pure gas is used, this approach may lead to errors if gas-side mass transfer resistance becomes appreciable.

The liquid-side mass transfer coefficients in the gas-liquid Taylor flow have been extensively studied, as well as the active mass transfer area (Dietrich et al., 2013; Sobieszuk et al., 2008; Shao et al., 2010; Sobieszuk et al., 2012; van Baten and Krishna, 2004; Yue et al., 2007). However, there are practically no data on the gas-side mass transfer coefficient, and therefore it is not clear whether and when neglecting the gas-side mass transfer resistance is justified.

*Corresponding author, e-mail: p.sobieszuk@ichip.pw.edu.pl

In this work data on the gas-side mass transfer coefficient in the Taylor flow in a closed microchannel are determined using numerical simulations, and discussion of the contribution of liquid- and gas-side mass transfer coefficients to the overall mass transfer coefficient in Taylor flow in a microreactor is presented.

2. CFD SIMULATIONS

3-D numerical simulations were performed using COMSOL 3.5, a commercial CFD package. Mesh was generated automatically, and contained depending on the case, from about 40000 to 200000 tetrahedral elements. A schematic view of the microreactor channel is shown in Fig. 1. The channel had a circular cross section of internal diameter 0.4 mm. Simulations were performed in the coordinate system fixed to the bubble. The modelled domain included a sector of the channel filled with liquid with a single gas bubble (Fig. 1).

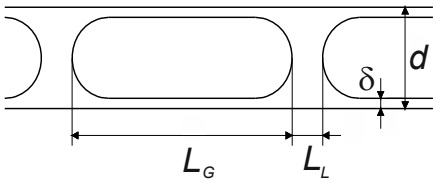

Fig. 1. Scheme of Taylor flow

The aim of this study was to determine the values of the gas-side mass transfer coefficient, and not to simulate the performance of a particular microreactor. We therefore pre-determined the shape of a bubble (on the basis of earlier studies), and neglected any phenomena other than mass transfer (like heat transfer accompanying mass transfer, or bubble shape changes caused by gas compressibility). These effects may of course appear in a real process, but they do not change the value of mass transfer coefficient (although they do influence the mass transfer rate). The following assumptions were therefore made:

A1 The shape of the bubble was defined as a cylinder with two hemispheres at both ends. This was based on high-speed photographs of the Taylor flow, taken in a previous study (Ilnicki et al., 2009).
A2 Mass transfer takes place by evaporation of a liquid into the gas bubble. The physicochemical parameters of the gas (unless stated otherwise) were those of nitrogen, and of the liquid – those of ethanol.
A3 No mass transfer limitations in the liquid phase (zero mass transfer resistance in the liquid phase).
A4 Liquid and gas are incompressible.
A5 The thickness of the liquid layer between the gas bubble and the reactor wall has been chosen arbitrarily δ=10 μm (Aussillous and Quéré, 2000; Bretherton, 1961). This value corresponds to the capillary number values in the range from $3\cdot10^{-3}$ to $26\cdot10^{-3}$.

The process of forming of the bubble was not considered in this work.

2.1. Model description

To analyse mass transfer between a gas bubble and the surrounding liquid it is necessary to determine the velocity field in the domain considered by solving the Navier - Stokes (N-S) equation system (1):

$$\begin{aligned} &\rho U \cdot \nabla U = \nabla \cdot [-pI + \mu (\nabla U + (\nabla U)^T)] \\ &\nabla \cdot U = 0 \end{aligned} \tag{1}$$

Considering that the analysis is performed in a coordinate system linked to the bubble, the velocity field must be generated by the interaction of the moving side wall of the channel with an initially stationary liquid, and extended into the fixed bubble. In the problem considered, the hydrodynamic study can be performed separately for the liquid phase and the gas phase.

To determine the concentration field it is necessary to solve the mass transfer Eq. (2):

$$\frac{\partial c}{\partial t} + \nabla \cdot (-D \nabla c) = U \cdot (-\nabla c) \tag{2}$$

However, considering assumptions A2 and A3, it is sufficient to do it for the gas phase only. The boundary conditions for the liquid phase are explained in Fig. 2 and Tab. 1. For the gas phase the boundary conditions are explained in Fig. 3 and Tab. 2. Initial conditions used in calculations are shown in Tab. 3.

Table 1. Liquid phase boundary conditions for Eq. (1)

	Liquid phase boundary conditions for Eq. (1)
B1 – moving (sliding) wall	$n \cdot U_L = 0$ $U_L \cdot t_a = u_b$
B2 – inlet/outlet	$\mu\left(\nabla U_L + (\nabla U_L)^T\right) n = 0$
B3 – bubble surface liquid-side	$n \cdot U = 0$ $t_a \cdot \left(-pI + \mu\left(\nabla U_L + (\nabla U_L)^T\right)\right) n = 0$

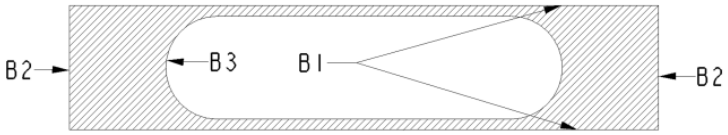

Fig. 2. Gas phase boundary conditions for Eqs. (1)-(2)

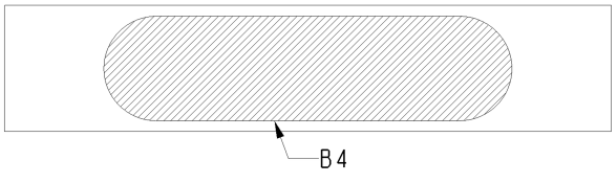

Fig. 3. Gas phase boundary conditions

Table 2. Gas phase boundary conditions for Eqs. (1)-(2)

	Gas phase conditions boundary for Eqs. (1) and (2)
B4 – moving bubble surface gas-side, Eq. (1)	$n \cdot U_G = 0$ $U_G \cdot t_a = U_L$
B4 – concentration, Eq. (2)	$c = c^*$

Table 3. Initial conditions for Eqs. (1)-(2)

	Initial conditions
Eq. (1)	$t = 0 \Rightarrow U_L = 0 \; and \; U_G = 0$
Eq. (2)	$t = 0 \Rightarrow c = 0$

Fig. 4 shows exemplary velocity field.

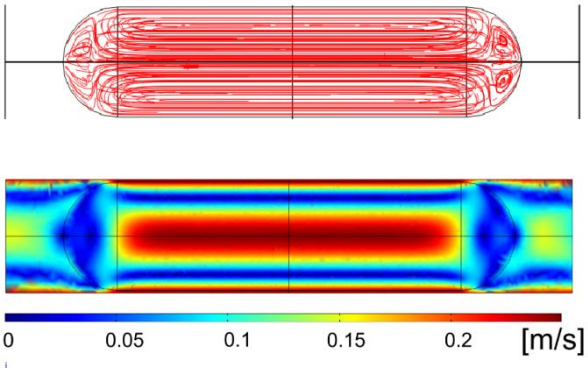

Fig. 4. Sample simulation results, velocity field;
L_G=2.25·10^{-3} [m,] d=5·10^{-4} [m], D_G=10^{-5} [m^2/s], u_b=0.26 [m/s], v_G=1.5·10^{-5} [m^2/s]

At the beginning of the vaporisation process the vapour concentration in the bubble equals zero. The concentration increases with time until saturation concentration is reached. The simulations give the vapor concentration values for different points within the bubble and different time values. From these concentration fields the average (integrated over the bubble volume) concentration of the liquid vapour in the nitrogen bubble was calculated as a function of time *c(t)*. Fig. 5 shows sample simulation results - vapour liquid concentration fields for six different values of time.

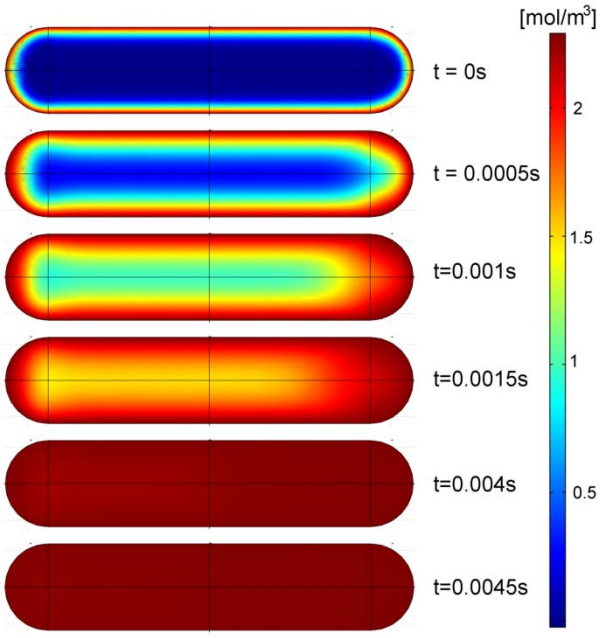

Fig. 5. Sample simulation results - concentration fields of the vapour of evaporating liquid for six different values of time; L_G=2.25·10^{-3} [m,] d=5·10^{-4} [m], D_G=10^{-5} [m^2/s], u_b=0.26 [m/s], v_G=1.5·10^{-5} [m^2/s]

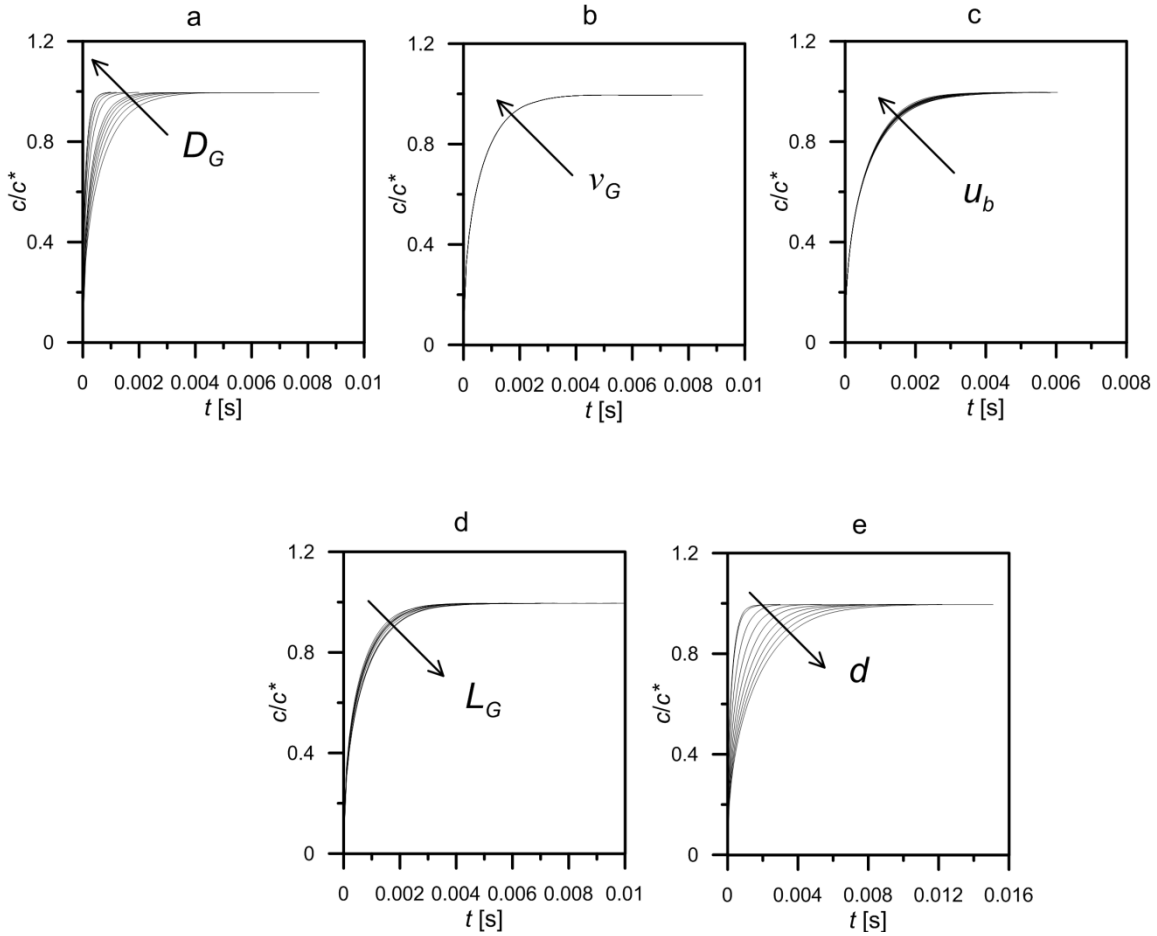

Fig. 6. Concentration profiles for all simulations

Five series of simulations were carried out. The influence of gas phase diffusivity (D_G), gas phase kinematic viscosity (ν_G), microchannel diameter (d), bubble slug length (L_G) and bubble velocity (u_b) on the gas-side mass transfer coefficients was determined. The ranges of the variables were: D_G=1·10^{-5}÷6·10^{-5} [m^2/s]; ν_G=1·10^{-6}÷2.2·10^{-5} [m^2/s]; d=0.2·10^{-3}÷10^{-3} [m]; L_G=8·10^{-4}÷2·10^{-3} [m]; u_b=0.06÷0.5 [m/s]. These ranges are limited to the region where Taylor flow is obtainable. The results of simulations are shown in Fig. 6. Fig. 7 shows the way the saturation time t_S has been determined. It was defined as the time when c=0.999c*.

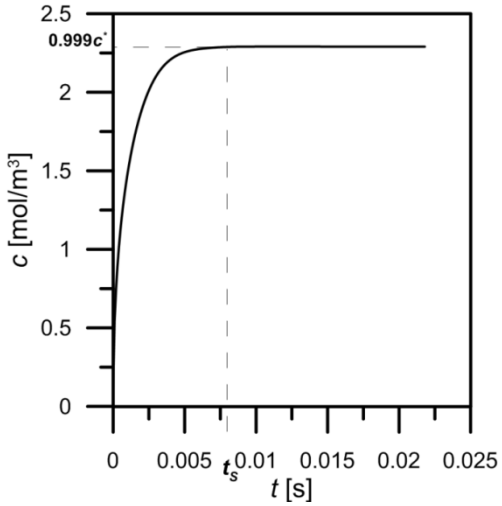

Fig. 7. A sample concentration profile

A mass balance of the vapour contained in the bubble was made:

$$V\frac{dc}{dt} = k_G\left(c^* - c(t)\right)F \tag{3}$$

and, using *c(t)* profile, the gas-side mass transfer coefficient was found:

$$k_G = \frac{\frac{V}{F}\int_0^{0.999\,c^*}\frac{dc}{c^* - c(t)}}{t_S} \tag{4}$$

As may be seen from Fig. 6, the time necessary for saturation is very low (of the order of 0.01 [s]). For the bubble velocity of the order of 0.5 [m/s], one can expect saturation to occur at the distance of about 5 [mm] from the inlet channel.

3. RESULTS AND DISCUSSION

Figs. 8a-8e show k_G values as functions of a single variable: D_G, v_G, u_b, L_G, d respectively. One can see that the values of the gas-side mass transfer coefficient depend significantly on gas diffusivity and microchannel diameter, whereas the influence of bubble length, gas viscosity and bubble velocity on the k_G values is much weaker. In order to estimate the relative importance of gas-side mass transfer, one has to recall the classical equation:

$$\frac{1}{K_L} = \frac{1}{k_L} + \frac{HRT}{k_G} \tag{5}$$

for physical absorption, and

$$\frac{1}{K_L^*} = \frac{1}{E\,k_L} + \frac{HRT}{k_G} \tag{6}$$

for absorption accompanied by a chemical reaction. In the above equations H denotes the Henry's constant, and E is the enhancement factor. The enhancement factor E can assume values of the order of 10^0 to10^2 (Danckwerts, 1970).

In the following discussion an average value of gas-side mass transfer coefficient k_G = 0.4 [m/s] was assumed. Liquid-side mass transfer coefficient was estimated based on the Higbie's model (Higbie, 1935):

$$k_L = 2\sqrt{\frac{D_L}{\pi\,\tau}} \tag{7}$$

where τ is the so-called "Higbie's contact time", i.e. the time of the contact of both phases. The same Higbie's time values for both phases are assumed, thus:

$$\frac{k_G}{k_L} = \sqrt{\frac{D_G}{D_L}} = \sqrt{\frac{10^{-5}}{10^{-9}}} = 100 \tag{8}$$

where D_G and D_L are diffusivity of gas and liquid phase respectively. Thus, for k_G=0.4 [m/s], coefficient k_L equals k_L=0.004 [m/s] (experimental values of k_L range from $0.2\cdot10^{-3}$ to $1.3\cdot10^{-3}$ [m/s] (Yue et al., 2007; Sobieszuk et al., 2011)). Fig. 9 shows the influence of both mass transfer coefficients, for different H values, on the absorption rate in the case of physical absorption (Eq. (5)).

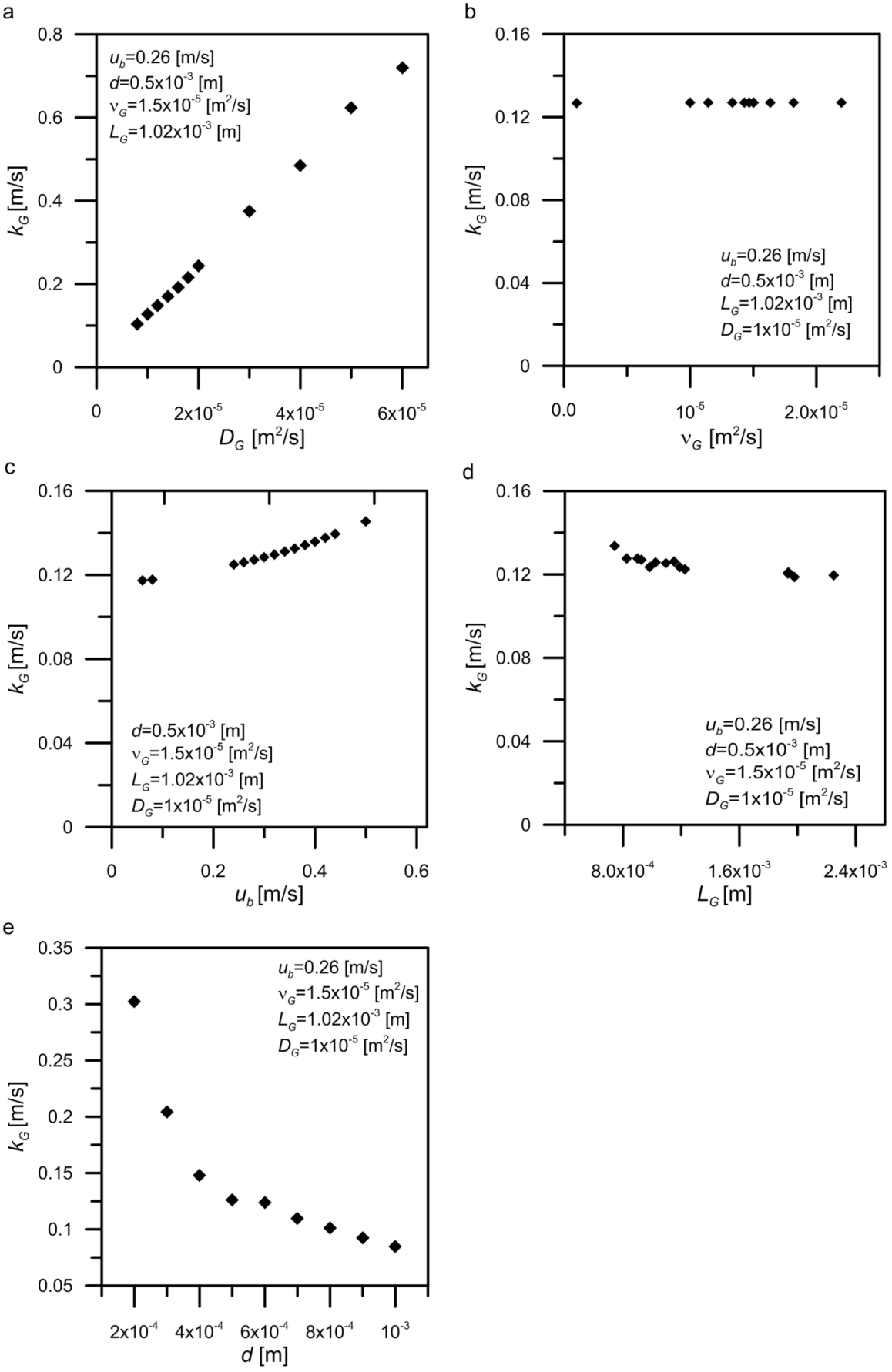

Fig. 8. Dependences of the gas-side mass transfer coefficient on: (a) diffusivity, (b) kinematic viscosity, (c) gas bubble velocity, (d) gas bubble length, (e) microchannel diameter

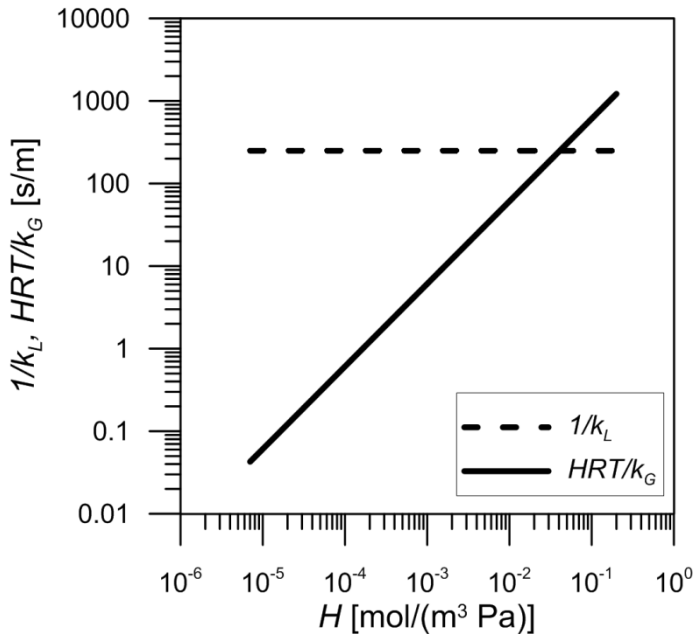

Fig. 9. The contributions of liquid- and gas-side mass transfer coefficients to the overall mass transfer coefficient in physical absorption

For gases having low solubility in liquids (e.g. O_2), liquid-side resistance predominates. However, an increase in gas solubility causes an increase of the contribution of the gas-side mass transfer resistance which, in the end, can be even higher than the liquid-side resistance. This situation is observed for ammonia-water system. It should therefore be remembered that in such cases of physical absorption and diluted gas systems the gas-side mass transfer resistance should be taken into account.

Situation is similar when we are dealing with chemical absorption. Fig. 10 shows dependencies of both resistances as functions of the enhancement factor (E) for low and high Henry's constant values.

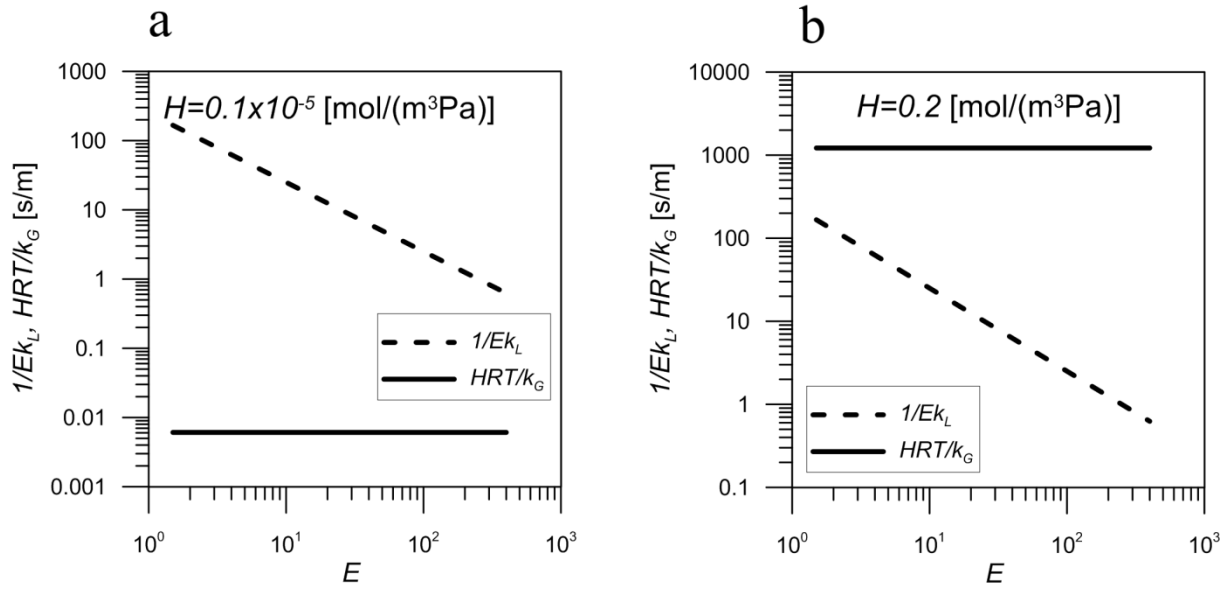

Fig. 10. The contributions of liquid- and gas-side mass transfer coefficients to the overall mass transfer coefficient in chemical absorption for low (a), and high values of Henry's constant (b)

As can be seen, for slightly soluble gases, even for fast reaction, the contribution of gas resistance is small (Fig. 10a). On the other hand, for highly soluble gases and chemical absorption the gas-side mass

transfer resistance contribution is always predominant (Fig. 10b). The situation is more complicated for gases of medium solubility (Fig. 11a).

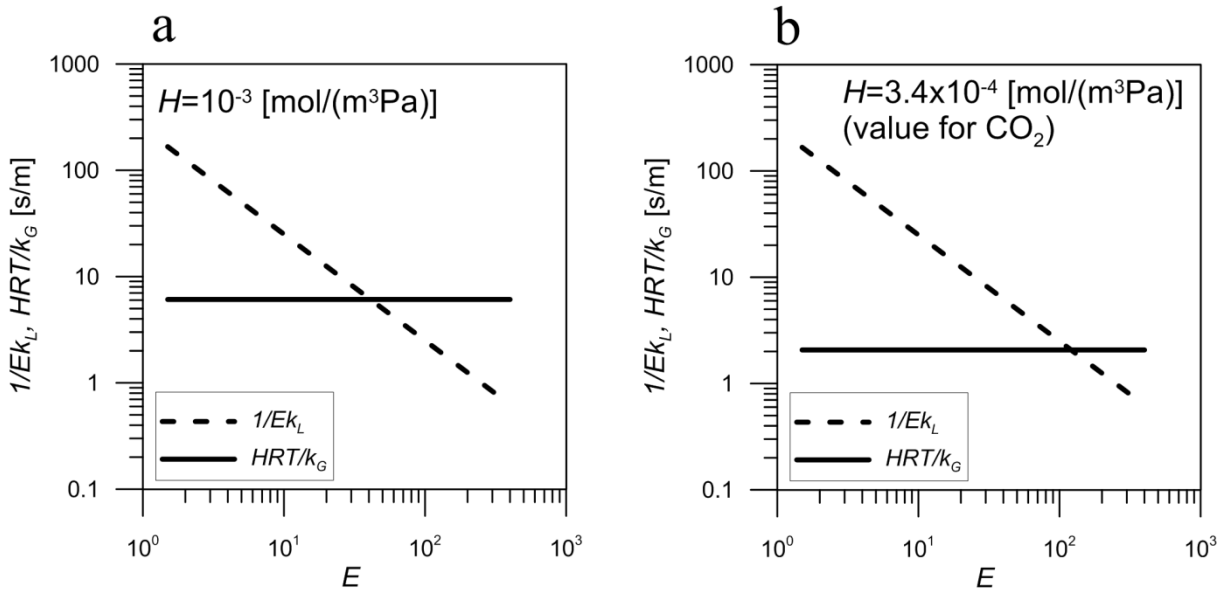

Fig. 11. The contributions of liquid- and gas-side mass transfer coefficients to the overall mass transfer coefficient in chemical absorption, (a) average values of Henry's constant, (b) absorption of CO_2, H=3.4x10^{-4} [mol/(m^{3}Pa)] (Fogg and Gerrard, 1991)

A gas commonly used for absorption rate investigations, carbon dioxide, belongs to this category. It is usually absorbed into different reactive solutions (e.g. NaOH or amine water solutions). Because of the relatively low CO_2 solubility, the gas-side mass transfer resistance is usually neglected. As can be seen from Fig. 11b this approach in not always correct. For fast chemical reactions, mass transfer resistances are comparable and the gas-side resistance may be significant. Therefore, neglecting the gas-side coefficient may lead to errors in experimental data interpretation.

4. CONCLUSIONS

The gas-side mass transfer from gas bubbles during the Taylor flow in a microchannel was investigated using the 3D numerical simulation method. The influence of gas diffusivity, gas viscosity, channel diameter, bubble length and bubble velocity was independently determined. The results revealed a strong influence of gas diffusivity and channel diameter on the value of the gas-side mass transfer coefficient and weak influence of the gas viscosity, bubble length and bubble velocity on this value. The problem of gas-side mass transfer contribution in the overall mass transfer coefficient has been discussed. It has been shown that in some cases the gas-side resistance to mass transfer may be significant, and neglecting it may lead to errors in the interpretation of measurement results of the mass transfer rate.

This work was in part supported by the budget sources for The National Centre for Science (Poland), Grant No. N N209 026140.

SYMBOLS

c liquid vapor concentration, mol/m^3

c^*	saturation concentration, mol/m^3
D	diffusivity, m^2/s
E	enhancement factor,-
F	gas bubble surface, m^2
H	Henry's constant, mol/(m^3 Pa)
I	unit vector,-
K	overall mass transfer coefficient, m/s
K^*	overall mass transfer coefficient witch chemical reaction, m/s
k_G	gas-side mass transfer coefficient, m/s
k_L	liquid-side mass transfer coefficient, m/s
L_G	gas bubble length, m
L_L	liquid slug length, m
n	normal vector,-
p	pressure, Pa
R	gas constant, J/(mol K)
T	temperature, K
t	time, s
t_a	tangential vector,-
t_s	"saturation" time, s
U	velocity vector, m/s
u_b	bubble velocity, m/s
V	gas bubble volume, m^3
d	channel diameter, m

Greek symbols

δ	liquid film thickness, m
μ	dynamic viscosity, Pa s
ν	kinematic viscosity, m^2/s
ρ	density, kg/m^3
τ	Higbie's contact time, s

Subscripts

G	gas phase
L	liquid phase

REFERENCES

Abolhasani M., Singh M., Kumacheva E., Günter A., 2012. Automated microfluidic platform for studies of carbon dioxide dissolution and solubility in physical solvents. *Lab Chip*, 12, 1611-1618. DOI: 10.1039/c2lc21043f.

Aussillous P., Quéré G., 2000. Quick deposition of a fluid on the wall of a tube. *Physics Fluids*, 12, 2367−2371. DOI: 10.1063/1.1289396.

Bretherton F.P., 1961. The motion of long bubbles in tubes. *J. Fluid Mechanics*, 10, 166−188.

Chambers R.D., Holling D., Spink R.C.H., Sandford G., 2001. Elemental fluorine Part 13. Gas–liquid thin film microreactors for selective direct fluorination. *Lab Chip*, 1, 132-137. DOI: 10.1039/B108841F.

Churski K., Korczyk P., Garstecki P., 2010. High-throughput automated droplet microfluidic system for screening of reaction conditions. *Lab Chip*, 10, 816-818. DOI: 10.1039/B925500A.

Danckwerts P.V., 1970. *Gas-liquid reactions*. McGraw-Hill, New York.

Dietrich N., Loubiere K., Jimenez M., Hebrard G., Gourdon C., 2013. A new direct technique for visualizing and measuring gas-liquid mass transfer around bubbles moving in straight millimetric square channel. *Chem. Eng. Sci.*, 100, 172-182. DOI: 10.1016/j.ces.2013.03.041.

Ehrich H., Linke D., Morgenschweis K., Baerns M., Jahnish K., 2002. Application of microstructured reactor technology for the photochemical chlorination of alkylaromatics. *Chimia*, 5, 647-653.

Fogg P.G.T., Gerrard W., 1991. *Solubility of gases in liquids*. Wiley, Chichester.

Higbie R., 1935. The rate of absorption of a pure gas into a still liquid during short periods of exposure. *Trans. Am. Inst. Chem. Engrs*., 35, 365-389.

Hessel V., Angelli P., Gavriilidis A., Lowe H., 2005. Gas−liquid and gas−liquid−solid microstructured reactors: contacting principles and applications. *Ind. Eng. Chem. Res*., 44, 9750–9769. DOI: 10.1021/ie0503139.

Ilnicki F., Sobieszuk P., Pohorecki R., 2009. Simulation of the two phase flow in a closed microchannel. *Chem. Proc. Eng*. 30, 205-216.

Lefortier S.G.R., Hamersma P.J., Bardow A., Kreutzer M.T., 2012. Rapid microfluidic screening of CO_2 solubility and diffusion in pure and mixed solvents. *Lab Chip*, 12, 3387-3391. DOI: 10.1039/c2lc40260b.

Shao N., Gavriilidis A., Angeli P., 2010. Mass transfer during Taylor flow in microchannels with and without chemical reaction. *Chem. Eng. J.*, 160, 873-887. DOI: 10.1016/j.cej.2010.02.049.

Sobieszuk P., Cygański P., Pohorecki R., 2008. Volumetric liquid side mass transfer coefficient in a gas – liquid microreactor. *Chem. Proc. Eng.*, 29, 651-661.

Sobieszuk P., Pohorecki R., Cygański P., Grzelka J., 2011. Determination of the interfacial area and mass transfer coefficients in the Taylor gas–liquid flow in a microchannel. *Chem. Eng. Sci.*, 66, 6048-6056. DOI: 10.1016/j.ces.2011.08.029.

Sobieszuk P., Aubin J., Pohorecki R., 2012. Hydrodynamics and mass transfer in gas-liquid flows in microreactors. *Chem. Eng. Technol.*, 35, 1346-1358. DOI: 10.1002/ceat.201100643.

van Baten J.M, Krishna R., 2004. CFD simulations of mass transfer from Taylor bubbles rising in circular capillaries. *Chem. Eng. Sci.*, 59, 2535-2545. DOI: 10.1016/j.ces.2004.03.010.

Yue J., Chen G., Yuan Q., Luo L., Gonthier Y., 2007. Hydrodynamics and mass transfer characteristics in gas-liquid flow through a rectangular microchannel. *Chem. Eng. Sci*., 62, 2096-2108. DOI: 10.1016/j.ces.2006.12.057.

Received 12 September 2013
Received in revised form 02 December 2013
Accepted 23 December 2013